PROCEEDINGS, 51st Workshop on Geothermal Reservoir Engineering
Stanford University, Stanford, California, February 9-11, 2026
SGP-TR-230

Recent Geyser-Like Eruption and Renewed Hydrothermal Activity in the Steamboat Geothermal Area, Nevada

Cary R. Lindsey[1], Owen Callahan[2], Rachel Micander[3], Nicole Hart-Wagoner[1], and Griffin Burke-Ruhl[3]

[1]Great Basin Center for Geothermal Energy, Nevada Bureau of Mines and Geology, University of Nevada Reno

[2]En Echelon Geosolutions

[3]Great Basin Science Sample and Records Library, Nevada Bureau of Mines and Geology, University of Nevada Reno

Keywords: geothermal surface manifestations, monitoring, thermal drone

ABSTRACT

On June 3, 2025, an uncapped, shallow (~15- 20 m), abandoned well south of Reno, Nevada, unexpectedly erupted, shooting boiling water nearly 30 m high, marking the first geyser-like activity documented at the site in decades. The eruption occurred on the lower sinter terrace in the Steamboat geothermal area, a site known historically for its dramatic surface expressions. Steamboat Springs was once home to some of the largest geysers in the United States, with abundant hot springs and fumaroles active into the early 1900s. Geysers diminished by the mid-20th century. Renewed changes were first noted in 2022, when steaming ground expanded and water began reappearing along fractures; activity steadily increased, culminating in the 2025 eruption.

Rather than treating the event solely as an isolated anomaly, we use it as a case study demonstrating the value of systematic, near-surface geothermal monitoring. Beginning in June 2025, we implemented an integrated monitoring program that combined water sampling and geochemical analyses, thermal drone surveys, continuous temperature logging, and detailed mapping of evolving surface features. These complementary tools allowed rapid characterization of fluid sources, heat distribution, and temporal changes in hydrothermal expression.

This study illustrates how relatively low-cost, field-deployable methods can provide actionable information for hazard assessment, resource management, and interpretation of dynamic geothermal behavior. The Steamboat eruption highlights both the persistence of shallow hydrothermal activity in developed fields and the importance of proactive monitoring to anticipate surface changes that may affect infrastructure, operations, and public safety.

1. INTRODUCTION

The Steamboat geothermal area (Steamboat), located at the southern edge of Reno, Nevada, is one of the most historically significant and active hydrothermal fields in the western United States. The field has a long record of geothermal activity, beginning with Indigenous use and later becoming widely known in the nineteenth century for its remarkable geysers, hot springs, and steaming ground. Steamboat was once home to the third largest geyser in the United States. This feature persisted until the early 1900s when a large regional earthquake and associated hydrologic changes altered the flow regime and caused major geysering to cease (White, 1968). Although large eruptions stopped more than a century ago, surface manifestations including hot pools, fumaroles, warm ground, and silica sinter deposits continue to reflect active hydrothermal circulation beneath the area. Today, Steamboat supports a mix of uses that include a long-established resort and spa complex that relies on natural hot water, as well as nearby industrial geothermal power production. These land uses coexist with historic and natural surface features that remain important parts of the local hydrologic and cultural landscape.

In recent years, residents, landowners, and scientists have observed a gradual intensification of surface hydrothermal expressions across parts of the Steamboat area. Beginning around 2022, several locations displayed expanding steaming ground, warmer temperatures, and intermittent shallow seepage along natural fractures and older anthropogenic features. Local residents contacted the Nevada Bureau of Mines and Geology (NBMG), and the activity was documented through repeated site visits and measurements. These changes were subtle at first but became increasingly noticeable through 2023 and early 2025. Variability of this type can occur naturally in dynamic hydrothermal systems influenced by complex fault networks and seasonal groundwater interactions. Even so, the elevated visibility of these features prompted community interest and encouraged a more systematic effort to document and understand the changes that were underway.

This period of heightened attention reached a peak on June 3, 2025, when an uncapped shallow pipe, of unclear origin, briefly discharged boiling water and steam nearly 30 meters into the air. The event was short and caused no injuries or property damage, but it represented the first geyser-like activity documented in the area in many decades. Because the eruption originated from a legacy feature rather than a natural vent, and because shallow hydrothermal systems can experience rapid shifts in permeability, pressure, and flow pathways, the event highlighted the importance of sustained monitoring in areas where natural processes, historic infrastructure, and active land use are closely integrated.

In response, NBMG initiated a multi-method monitoring program to document surface activity, characterize shallow hydrologic and thermal patterns, and establish a quantitative baseline for interpreting future changes. These efforts include repeated drone-based thermal surveys, installation of continuous temperature loggers, systematic mapping of surface features, water and gas sampling, and photographic

documentation of evolving conditions. The goal of this work is not to assign causes or evaluate the performance of geothermal operations. Instead, the objective is to develop a clear, reproducible scientific record of surface hydrothermal behavior through time. Tracking flow paths, temperature variability, and fluid sources helps explain how shallow hydrothermal systems respond to changing subsurface conditions in an active, fault-controlled environment. This monitoring framework also supports communication with landowners, operators, and the broader public.

This paper presents the historical context of the Steamboat geothermal area, describes recent observations including the June 2025 eruption, and summarizes the monitoring approaches and early results collected by NBMG. The intent is to provide well-documented, repeatable observations that contribute to a longer-term dataset and support the case for continued monitoring of shallow hydrothermal systems, particularly in settings where historic infrastructure and modern land use intersect with active geothermal processes.

2. GEOLOGIC AND HYDROTHERMAL SETTING

The Steamboat geothermal area is located within the northern Walker Lane, a zone of active transtensional deformation that overlaps the broader Basin and Range province. The Walker Lane accommodates a substantial component of dextral shear between the Pacific and North American plates and is characterized by northwest-striking fault systems that transition northward into extensional structures in the northwestern Great Basin (Faulds et al., 2005; Jayko, 2012). This tectonic regime produces dense, intersecting fault and fracture networks that enhance crustal permeability and commonly localize geothermal upflow, as documented for numerous geothermal systems throughout western Nevada (Faulds et al., 2005; Siler, 2017).

At Steamboat, interlayered volcanic and volcaniclastic rocks, intrusive bodies, and sedimentary deposits create strong permeability contrasts and compartmentalization within the shallow crust (White et al., 1964; Silberman et al., 1979). These structural and lithologic controls have sustained a long-lived hydrothermal system that transports hot water and steam to shallow depths, where fluids ascend along faults and fractures to produce fumaroles, hot pools, silica sinter mounds, and areas of warm ground. Surface expressions have varied through time in response to changes in tectonic strain, groundwater levels, and evolving permeability pathways that regulate fluid ascent from deeper reservoirs (White, 1968; Silberman et al., 1979). This regional and stratigraphic framework provides important context for interpreting the recent activity and monitoring results described in this study.

2.1 Regional Geologic Context

Locally, the Steamboat field is controlled by steeply dipping fault zones that segment the volcanic and sedimentary sequence and focus fluid flow into discrete conduits. Channelized circulation along these structures allows thermal fluids to repeatedly access the shallow subsurface, sustaining persistent surface manifestations such as sinter terraces, hot pools, and steaming ground (White et al., 1964; White, 1968). The interaction between fault architecture and heterogeneous lithology therefore governs both the location and temporal variability of hydrothermal discharge observed at the site.

2.2 Surface and Subsurface Hydrothermal Influences

The hydrothermal system at Steamboat is fractured, with deep fluid ascent concentrated along major faults and subsidiary fractures that transmit heat and mass upward through the crust (White et al., 1964; White, 1968). Upflow commonly transitions through boiling and steam-rich zones that influence near-surface fluid chemistry and discharge characteristics. At shallow depths, geothermal fluids frequently mix with cooler meteoric groundwater, producing a range of thermal expressions that can migrate spatially and temporally as permeability evolves (White, 1968).

Historical descriptions of Steamboat document large geysers, vigorously boiling pools, and extensive steaming areas during the late nineteenth and early twentieth centuries, followed by periods of diminished activity (White, 1968). Silica sinter mounds and hydrothermal alteration deposits preserved at the surface provide evidence of long-term variability in discharge intensity and vent locations (White et al., 1964; Silberman et al., 1979). During renewed observations in the mid-1980s, eruptive activity was again documented at numerous vents but was concentrated primarily on the main sinter terrace west of U.S. 395; visits to the lower terrace identified only a single small spouter and no significant geysering, representing the only reported activity in that area at the time (Koenig, 1989). More recent observations from field investigations, remote sensing, and repeat site visits indicate that hydrothermal circulation remains active and continues to respond to both tectonic and hydrologic influences. Contemporary studies of surface thermal features at Steamboat and analogous systems emphasize the importance of integrating geologic framework, surface mapping, and monitoring datasets to interpret evolving discharge patterns and protect sensitive hydrothermal features (Huntington, 2010; Skalbeck et al., 2002; Kreuzer et al., 2024).

Human use of the Steamboat area also contributes to the present-day landscape. Development since the late nineteenth century has included drilling of shallow wells, construction of resort and spa facilities, and installation of infrastructure to access thermal waters. Legacy wells and pipes locally intersect shallow hydrothermal zones and may act as artificial conduits or vents when pressure or temperature conditions change. These anthropogenic features add an additional layer of complexity when interpreting modern surface activity.

Together, the regional tectonic framework, the structural and lithologic controls on permeability, the active hydrothermal system, and the history of human modification create a complex setting that explains both the persistence and variability of surface geothermal expressions

at Steamboat. These interactions have made Steamboat an important natural laboratory and case study for geothermal processes and surface-thermal-feature management in the western United States (White, 1968; Faulds et al., 2005; Kreuzer et al., 2024)

.3. OBSERVATIONS OF RENEWED HYDROTHERMAL ACTIVITY

Surface activity at the Steamboat geothermal field increased measurably between 2023 and 2025, evolving from diffuse steaming to focused, high-discharge features and ultimately a brief geyser-like eruption. Repeat site visits, mapping, temperature measurements, and fluid sampling document a stepwise escalation rather than a single abrupt event.

In 2023, changes were first noted as an expansion of steaming ground across the lower sinter terrace. Areas that had previously been dry or only weakly warm developed persistent vapor flux and moist, thermally altered soils. Steaming extended laterally along existing fractures and terrace margins, and faint sulfur odors and condensate staining became more widespread. No focused vents or flowing water were observed at this stage, and activity was primarily diffuse. By 2024, the character of activity shifted from diffuse degassing to localized venting. Several small seeps and weak springs appeared along fracture-controlled zones and at the base of the sinter mound where only steaming had been present the previous year. Surface temperatures measured at these features were elevated relative to surrounding ground and discharge became intermittently visible as splashing or “spitting” behavior. These observations marked the first evidence of shallow boiling and focused upward flow rather than broad vapor leakage.

During this period, the aerial extent of warm ground also increased, and repeated visits documented persistence of features rather than short-lived pulses, suggesting sustained pressurization of the shallow system.

In early 2025, existing vents became more energetic. Intermittent splashing intensified, small pools formed and drained repeatedly, and localized discharge points migrated along nearby fractures. Thermal drone surveys and ground measurements indicated continued concentration of heat and fluid flow into discrete pathways. The system exhibited greater temporal variability, with observable changes occurring over days to weeks rather than months.

Activity culminated in mid-June 2025, when an uncapped, shallow (~15–20 m) pipe began episodically discharging boiling water and steam, producing short-lived vertical jets (Figure 1). The eruption briefly generated a geyser-like column of water and vapor before the pipe was capped. Following capping, discharge did not cease but instead shifted laterally, with new small springs and persistent spitting vents forming along adjacent fractures and sinter surfaces. This redistribution indicates that the eruption reflected release of pressure along one conduit within a broader, actively pressurized shallow system.

After the pipe was sealed, several small perpetual spouters developed along the northern margin of the sinter mound and have persisted through subsequent months. These features maintain standing pools, active microbial mats, and near-boiling water levels, with water visible within adjacent fissures approximately 0.5 m below the surface. Continued enlargement of at least one vent and sustained thermal discharge suggests ongoing shallow permeability enhancement and sustained hydrothermal flux rather than a return to pre-eruption conditions.

Overall, the progression from (1) expanded steaming in 2023, to (2) formation of discrete seeps and vents in 2024, to (3) vigorous focused discharge and geysering in 2025 demonstrates a clear escalation in near-surface permeability and hydrothermal flux.

Figure 1. a. Open-pipe geysering from an uncapped shallow well on the Lower Sinter Terrace, producing intermittent vertical steam and water discharge. b. Diffuse steaming ground with active silica precipitation, hydrothermal alteration, and thermophilic microbial mats. c. New perpetual spouters along sinter mound and small discrete vent in driveway.

4. Methods

4.1 Temperature Monitoring

Continuous temperature monitoring was conducted to quantify temporal variability in shallow hydrothermal discharge and to document evolving thermal conditions during the 2025 observation period. Eight autonomous temperature loggers (Elitech Tlog 10E, external temperature sensor) were deployed across a range of hydrothermal and background settings at the Steamboat site (Figure 2). All instruments recorded temperature at a fixed interval of five minutes, providing continuous, multi-month time series datasets.

Loggers were installed directly within active discharge pathways and along fluid flow routes to capture both high-temperature conduit conditions and mixed surface runoff. Initial deployments included placement within the uncapped pipe that exhibited geysering behavior, where temperatures were recorded following cessation of eruption until the pipe was capped. Additional sensors were installed in a culvert and runoff channel that conveyed fluids draining from the sinter terrace to characterize cooling and mixing during surface transport.

As surface activity evolved, several loggers were relocated to newly formed small vents and pools that developed along the margins of the sinter mound to monitor localized thermal fluctuations associated with these features. To provide environmental context and background comparison, supplementary loggers were placed in Steamboat Creek and within the Steamboat Resort holding tank.

Loggers were secured in place to minimize disturbance, checked during routine site visits, and periodically downloaded to maintain continuous records. These measurements provide high-frequency temperature observations that allow short-term fluctuations, sustained discharge trends, and seasonal changes in hydrothermal activity to be evaluated.

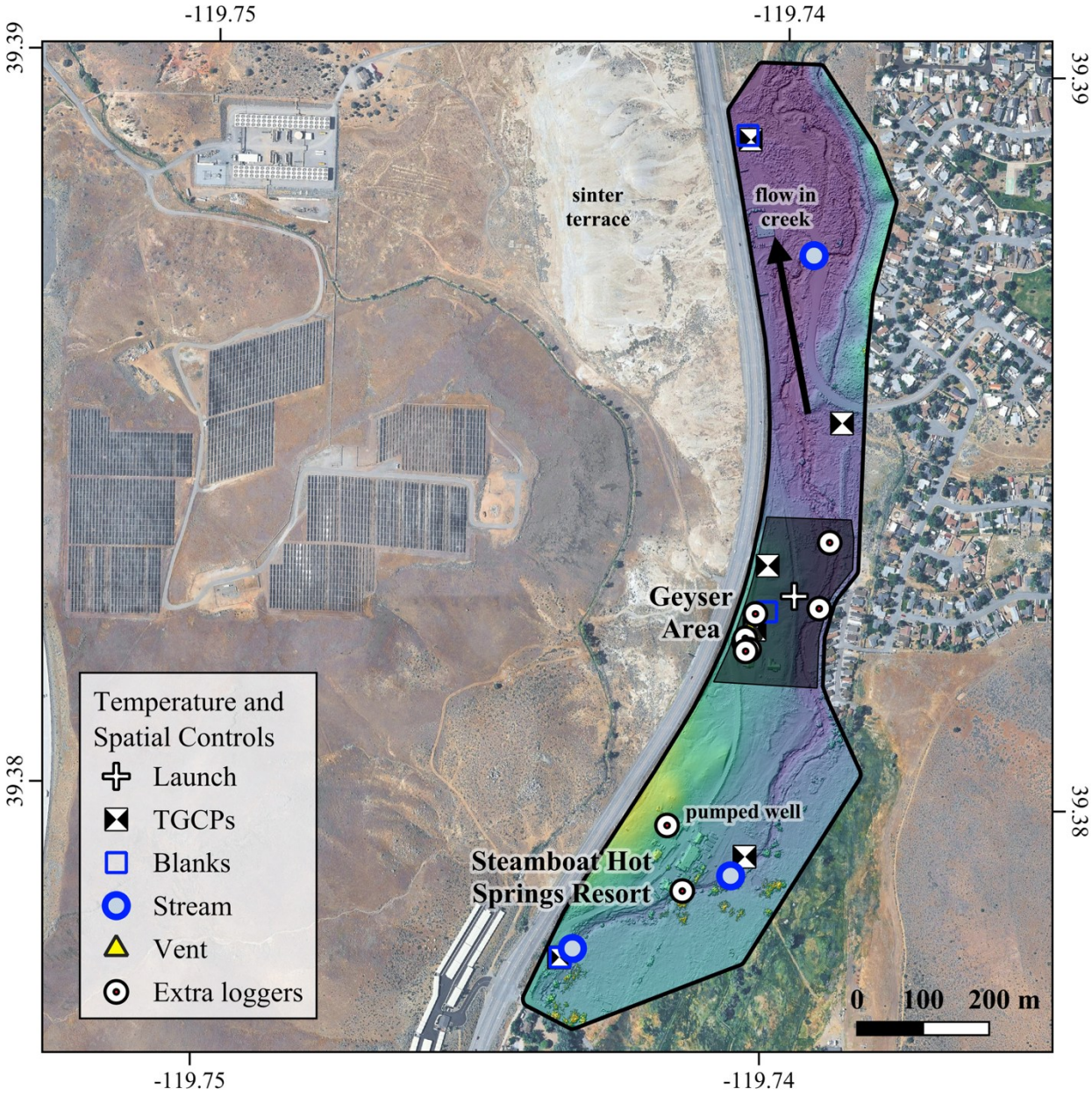

Figure 2. Drone flight areas and control points, including long-term temperature monitoring sites. The same 67 acres with persistent GPS-surveyed control points were flown with visible light and thermal drones in July and October along the north-flowing Steamboat Creek. The main geyser area, marked with the darker polygon, was also flown at low altitude (higher resolution). Steamboat Hot Springs Resort is located ~250 m SSW of the geyser area. Basemaps include Google Imagery and 2 cm DSM from visible light photogrammetry.

4.2 Drone-Based Thermography

Small drones are routinely used for land surveying and increasingly utilized in geoscience investigations (Westoby et al., 2012; Pavlis & Mason, 2017) from high resolution photogrammetry to geophysics and thermal mapping (e.g. Harvey et al., 2016; Müller et al., 2022; Zielinski et al., 2022; Brailo et al., 2024). Callahan and Hart-Wagoner (2025) reviewed three applications of thermal drones in geothermal science: exploration, characterization, and monitoring. In the present study, calibrated, drone-based thermal surveys were used for site characterization (mapping the extent and temperature of surface anomalies both known and previously unknown), and monitoring changes over time by repeating flight paths, control points, and processing methods in July and October 2025.

Nighttime calibrated thermal surveys were conducted on July 7-8th, and again on October 1st, 2025. The area of interest is roughly 0.27 km^2 (67 acres) with ground cover including bare earth and sinter with sparse vegetation, isolated trees, thick grasses and brush, and water, with some light infrastructure (hot spring resort, roads, businesses and dwellings, powerlines, billboards) (Figure 2).

Prior to flying, six instrumented Temperature Ground Control Points (TGCPs) were placed in the area of interest and surveyed with a BadElf Flex Mini Extreme with RTK connected over LTE. Error on these points is reported at 0.1 m horizontal and 0.15 m vertical. TGCPs were used for constructing structure-from-motion models and for tuning thermograms (described below). TGCPs and launch site for the October flights were placed on or near the same locations used for the June flights, with at least one stake left from the previous survey recovered at each site. All locations were resurveyed, with spatial differences between the June and October surveys <0.15 m horizontally and ≤0.07 m vertically (Table 1). Addition points of interest that would be easily recognized in the final imagery, including three water temperature locations in Steamboat Creek, a point-source fumarole in the driveway (Figure 1), and three ground temperatures within "blanks" marked with 1.5 m metal squares, where recorded but their locations not surveyed.

Table 1. Spatial differences between July and October ground control survey points.

Name	Δ Lat. (°)	Δ Long. (°)	Δ Elev. (m)	Instrument	Notes
TGCP1	0.0000004	-0.0000004	-0.03	Bad Elf Flex Mini Extreme RTK	1 stake (only 1 placed)
TGCP1	0.0000000	-0.0000004	-0.07	Bad Elf Flex Mini Extreme RTK	2 in good position
TGCP1	0.0000013	-0.0000023	-0.05	Bad Elf Flex Mini Extreme RTK	Both stakes found bent. Reinstalled.
TGCP1	0.0000002	0.0000002	-0.04	Bad Elf Flex Mini Extreme RTK	Both stakes found bent. Reinstalled.
TGCP1	0.0000001	-0.0000006	-0.07	Bad Elf Flex Mini Extreme RTK	2 in good position
TGCP1	0.0000003	-0.0000002	0.03	Bad Elf Flex Mini Extreme RTK	2 in good position
Launch	-0.0000001	-0.0000002	-0.05	Bad Elf Flex Mini Extreme RTK	Central stake in good position.
RTK Base	-0.0000001	-0.0000002	-0.053	Emlid Reach RS2+ PPK	Central stake in good position.

Thermal flights were conducted with a DJI Mavic 3T with an Emlid RS2+ base station and RTK units. The location of the base station was surveyed for several hours during site set-up, and the point was post-processed against known stations prior to flying. The corrected location was manually entered into the RTK unit, providing stable and consistent GPS-base locations for all flights.

Nighttime thermal flights were conducted at 50 m for thermal mapping, then the same area was flown with a higher resolution visible light camera at 53 m later that morning. A smaller region (0.03 km^2; 8 acres) most affected by recent changes was flown at 32 m (Table 2). The weather was mild during both visits, with ambient air temperature between 11-14 °C (52-57 °F), 51-60% relative humidity, and light to moderate wind speed (Table 3).

Thermal IR images were batch-tuned for each flight using DJI and ImageJ software (Irujo, 2022). Tuning parameters include distance, reflected (ambient) temperature, emissivity, and humidity. Tuning was conducted by processing imagery with known temperatures (TGCPs) and comparing the difference between measured and calculated temperatures. Images were then assembled into structure-from-motion models using Agisoft Metashape. Digital surface models (DSMs) and orthomosaics were exported and plotted in QGIS. The resolution of thermal orthomosaics is about 4-7 cm/pixel, and the resolution of visible light orthomosaics is about 2 cm/pixel. Actual ground sampling distance changes across the maps based on altitude above uneven topography. Distances between known points in the visible light and thermal surveys range from 5-13 cm in July and 5 to 20 cm in October. The vertical difference between points surveyed with BadElf GPS and the resulting DSMs is typically <1 m.

Table 2. Drone Flight Parameters

Flight	Drone	Area (km^2)	Area (acres)	Altitude (m)	Launch elevation (GPS) (m - WGS84 Ellispoidal)	Nominal flight elevation (m)	Speed (m/s)	Images	Nominal GSD (cm/px)	Front overlap (%)	Side overlap (%)	Tilt (deg)	Time (min)
TIR - July	Mavic 3T	0.27	67	50	1375.6	1425.6	4.2	4063	6.6	84	69	90	87
TIR-Z July	Mavic 3T	0.03	8	32	1375.6	1407.6	2.9	1295	4.2	85	72	90	25
VIS - July	Mavic 3T	0.27	67	53	1375.6	1428.6	5.5	1575	1.9	85	70	90	41
TIR - Oct	Mavic 3T	0.27	67	50	1375.6	1425.6	4.2	4039	6.6	84	69	90	87
TIR - Z Oct	Mavic 3T	0.03	8	32	1375.6	1407.6	2.9	1289	4.2	85	72	90	25
VIS - Oct	Mavic 3T	0.27	67	53	1375.6	1428.6	5.5	1560	1.9	85	70	90	41

Table 3. Flight Conditions

Flight	Date	Time Start (-7)	Time End (-7)	Wind speed Avg (Max) (m/s)	Ambient Air Temp. (°C) Kestrel	Ambient Air Temp. (°C) Elitech	R. Humidity (%) Kestrel	R. Humidity (%) Elitech	<1° C to Dew Point?
TIR	7/7/25	3:47 AM	5:31 AM	1.3 (2.9)	13.5 ±1.3	17.0 ±0.5	50.8 ±6.9	46.5 ±1.0	no
TIR - Zoom	7/8/25	5:19 AM	5:47 AM	1.0 (1.5)	13.3 ±1.4	12.1 ±0.4	55.5 ±7.7	61.7 ±2.4	no
VIS	7/7/25	7:09 AM	7:55 AM	-	-	-	-	-	-
TIR	10/1/25	4:38 AM	6:25 AM	2.3 (6.6)	13.8 ±1.0	13.0 ±0.9	53.5 ±2.9	58.5 ±2.7	no
TIR - Zoom	10/1/25	6:31 AM	6:56 AM	0.5 (1.3)	11.7 ±0.3	11.9 ±0.1	60.0 ±1.4	63.7 ±0.5	no
VIS	10/1/25	7:42 AM	8:27 AM	-	-	-	-	-	-

4.3 Aqueous Geochemistry

Two water samples were collected from active discharge features at Steamboat to characterize fluid chemistry. One sample (SBG001) was collected directly from the geysering pipe during active discharge, and a second (SBG002) was collected from a nearby runoff channel receiving overflow from the same feature. Samples were collected by hand in the field by the authors (C. Lindsey and N. Hart-Wagoner) and filtered on site through 0.45 µm filters to remove suspended particulates. Filtered samples were transferred to clean sample bottles, stored cool, and shipped to a commercial analytical laboratory for major-ion, trace-element, alkalinity, and dissolved silica analyses using standard laboratory methods

5. RESULTS

5.1 Temperature Logger Results

Although temperature monitoring was conducted across multiple hydrothermal and background settings, the records presented here focus on a representative subset of three loggers to illustrate contrasting thermal behavior across the lower terrace. These instruments were deployed in distinct hydrologic settings: (1) within the uncapped shallow well that had previously exhibited geysering, capturing near-reservoir conduit temperatures; (2) within an actively steaming fissure, representing shallow fracture-controlled upflow; and (3) within the Steamboat Resort holding tank as pumped fluid enters. Together, these locations span a gradient from focused, high-temperature upflow to cooled and mixed surface water and provide a clear comparison of thermal variability among different flow paths. Future work will expand monitoring in Steamboat Creek and incorporate fluid chemistry to further constrain mixing processes and subsurface connectivity. Figure 3 shows a representative segment of these records to illustrate the contrasting behaviors observed among the three sites.

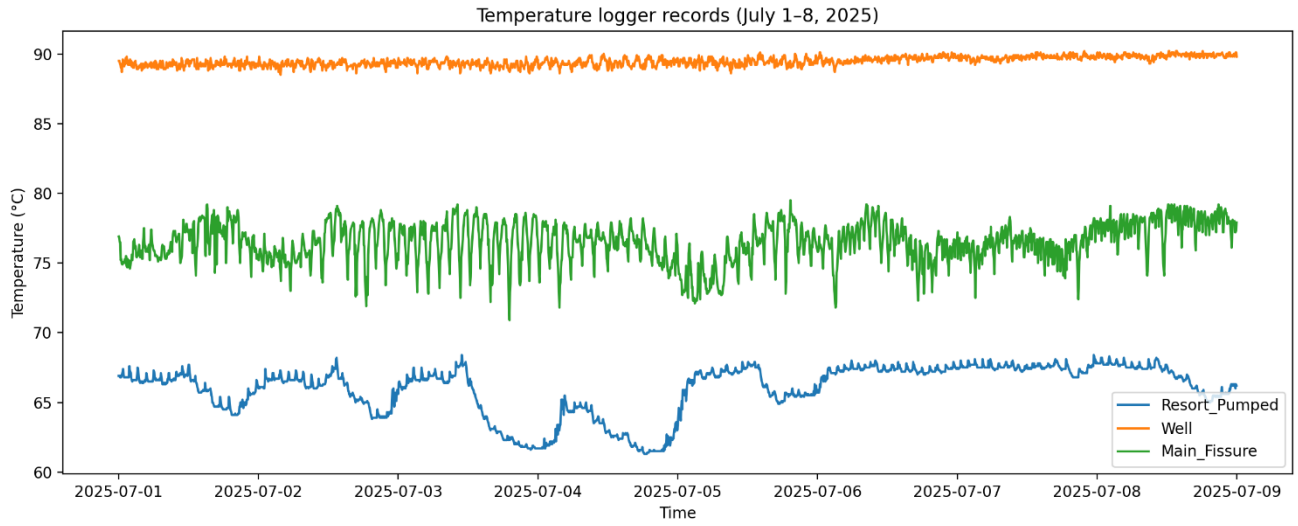

Figure 3. Representative temperature time series from three loggers deployed in an uncapped well, an actively steaming fissure, and the Steamboat Resort holding tank (1–8 July 2025).

5.2 Drone Thermal Imaging

Significant thermal anomalies identified in the drone imagery include steaming fissures associated with the new eruptive area, springs, warm ground and fissures near Steamboat Hot Springs Resort, warm seeps and hot springs within and around Steamboat Creek, and a hot flowing well at the very north end of the survey (Figure 4). Warm seeps and hot springs are found along most of the central part of the creek, on both banks, include some previously unmarked springs on the east bank. Around ~60 °C springs were later confirmed with field inspections. In both the July and October datasets, water temperature in the creek increases slightly with downstream distance, likely as a

result of accumulated thermal input. The water temperature in October is cooler than July, but the creek volume is lower and as a result the downstream warming effect is more pronounced.

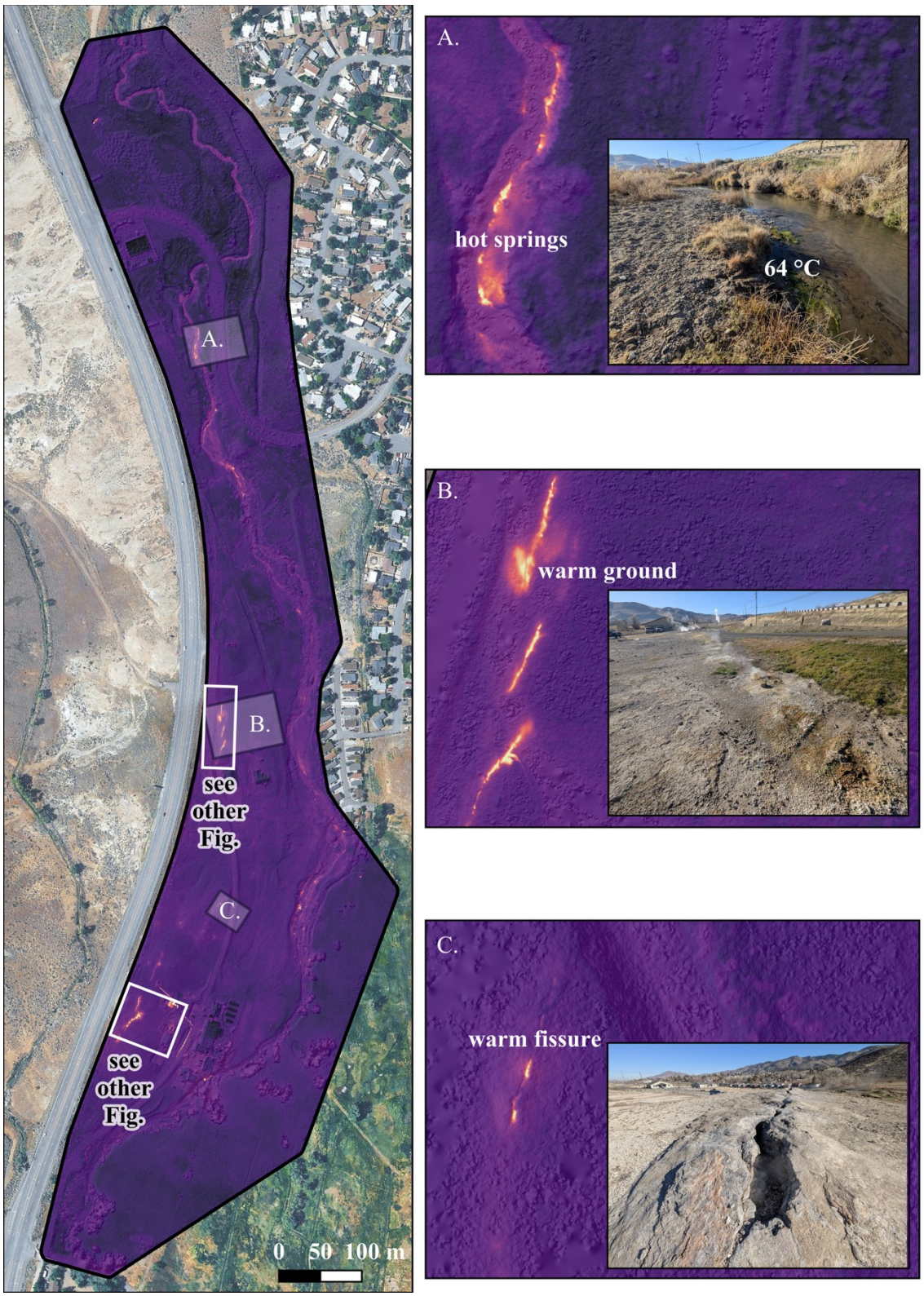

Figure 4. Results from the October sUAS thermal drone surveys. Multiple previously unrecognized and/or poorly located thermal features were identified in the thermal imagery. These features, including hot springs in Steamboat Creek, warm ground around incipient fissures, and warm "fossil" fissures, are generally persistent between July and October, although they do change in

magnitude. Differencing figures are shown in Figures 6 and 7 for the other areas of interest. The temperature scale is the same as in Figure 7.

There is good agreement between recorded and calculated temperatures at TGCPs in the thermal mosaics, with a a maximum difference of 1.3 °C in the larger dataset, and 1.0 °C in the lower altitude flight ("Zoom") (Table 4, Figure 5). Blanks are not used in calibration and show slightly warmer temperatures in the ground (~1-3 cm subsurface) than recorded at the surface by the TIR camera and mapped in the mosaics. Water in the creek appears ~3-5°C warmer than actually recorded. However, stream temperatures are compared between approximate locations, and some lateral temperature variation is expected at these sites. The largest difference between measured (logger) and calculated (mosaic) temperatures was observed at the vent in the driveway (Figure 1). This small point source was near boiling (80-90 °C), but is only 59-78 °C in the thermograms. This is likely due to pixel averaging across a small (cm-scale) anomaly. However, note that the measured and calculated temperature at this point source are 9 °C and 3.4 °C, respectively, cooler in October than July.

Table 4. Instrumented points used to tune and evaluate thermal orthomosaics.

Area	Name	Logger Number	Elevation (m)	Flight Elevation (m)	Distance (m)	Date	Fly Time	Ambient Temperature (°C)	Recorded Temperature (°C)	Calibrated Temperature (°C)	Difference (°C)
Steamboat	TGCP 1	29	1381.1	1425.6	44.5	7/7/25	4:41 AM	13.2	11.2	12.6	-1.4
Steamboat	TGCP 2	782	1380.3	1425.6	45.3	7/7/25	4:44 AM	11.6	13.1	12.8	0.3
Steamboat	TGCP 3	794	1376.3	1425.6	49.3	7/7/25	4:14 AM	15.2	6.3	6.8	-0.5
Steamboat	TGCP 4	783	1380.2	1425.6	45.4	7/7/25	3:50 AM	12.4	10.5	10.4	0.1
Steamboat	TGCP 5	781	1372.2	1425.6	53.4	7/7/25	4:59 AM	13.8	11.1	10.7	0.4
Steamboat	TGCP 6	785	1368.9	1425.6	56.7	7/7/25	5:23 AM	14.9	9.7	9.4	0.3
Steamboat	Blank 1	784	1379.6*	1425.6	46.0	7/7/25	4:43 AM	11.9	18.3	15.9	2.4
Steamboat	Blank 2	786	1379.9*	1425.6	45.7	7/7/25	3:51 AM	12.3	19.9	17.4	2.5
Steamboat	Blank 3	809	1368.7*	1425.6	56.9	7/7/25	5:24 AM	14.8	16.2	13.3	2.9
Steamboat	Vent	787	1381.7*	1425.6	43.9	7/7/25	4:41 AM	13.2	90.1	63.0	27.1
Steamboat	Water u	806	1376.4*	1425.6	49.2	7/7/25	3:52 AM	12.3	18.3	23.5	-5.2
Steamboat	Water m	810	1374.4*	1425.6	51.2	7/7/25	4:06 AM	15.1	18.6	23.1	-4.5
Steamboat	Water d	795	1368.0*	1425.6	57.6	7/7/25	5:16 AM	13.5	20.1	25.0	-4.9
Steamboat Zoom	TGCP 1	29	1381.1	1407.6	26.5	7/8/25	5:35 AM	14.6	11.0	12.6	-1.6
Steamboat Zoom	TGCP 2	782	1380.3	1407.6	27.3	7/8/25	5:25 AM	11.1	13.0	12.2	0.8
Steamboat Zoom	Blank 1	784	1379.6*	1407.6	28.0	7/8/25	5:32 AM	14.3	18.2	14.8	3.4
Steamboat Zoom	Vent	786	1381.7*	1407.6	25.9	7/8/25	5:36 AM	14.4	89.0	77.2	11.8

* from DSM

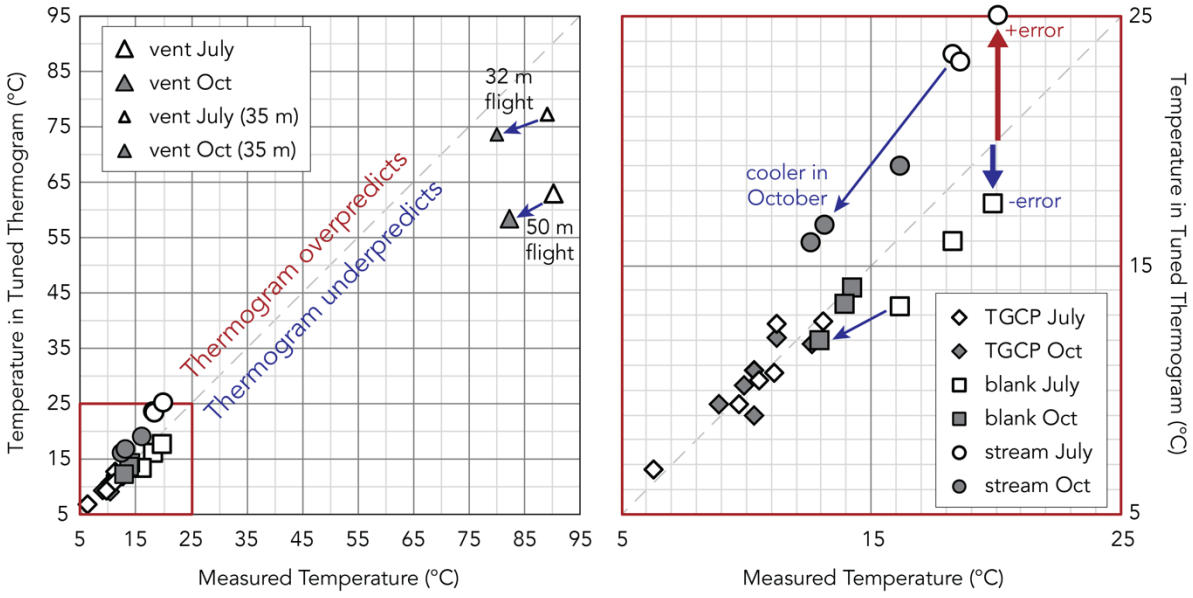

Figure 5. Measured temperatures versus results from thermal drone mapping in July and October. Thermograms were bulk tuned against six instrumented, high emissivity TGCPs, which are thus well fit to measured values. Surface ground temperatures were measured in three "blanks" and are warmer than indicated in the thermograms. Water temperatures measured in three locations in Steamboat Creek are all several degrees warmer in the thermograms than actually recorded. Large differences are observed at a small, point-source steaming vent near the main eruption. This underpredicted temperature is likely due to the

small size of the feature compared to pixel size (7 cm). Higher resolution flights show a better fit between measured temperatures and thermograms. Ground, water, and vent measures are all cooler in October relative to July.

The main thermal features identified in the July dataset (fissures, warm ground, warm springs in the creek) are apparent in the October dataset. Qualitatively, these features look very similar in magnitude and dimensions. However, because registration differences between TGCP locations in the thermal orthomosaics only differ by 2-18 cm between July and October, changes affecting areas larger than ~20 cm are discernible with raster math. Using this approach, a larger area of warm ground around the resort appears to be as much as 15 °C cooler in October than in July, and the main eruptive fissure appears cooler, except for at the northern tip of the two northern most fissures in the array (Figures 6 and 7). Some areas of the creek appear warmer, perhaps due to lower water levels in October revealing additional thermal discharge relative to stream water, while other areas that were already exposed in the July flights appear cooler, suggesting a decrease in thermal discharge.

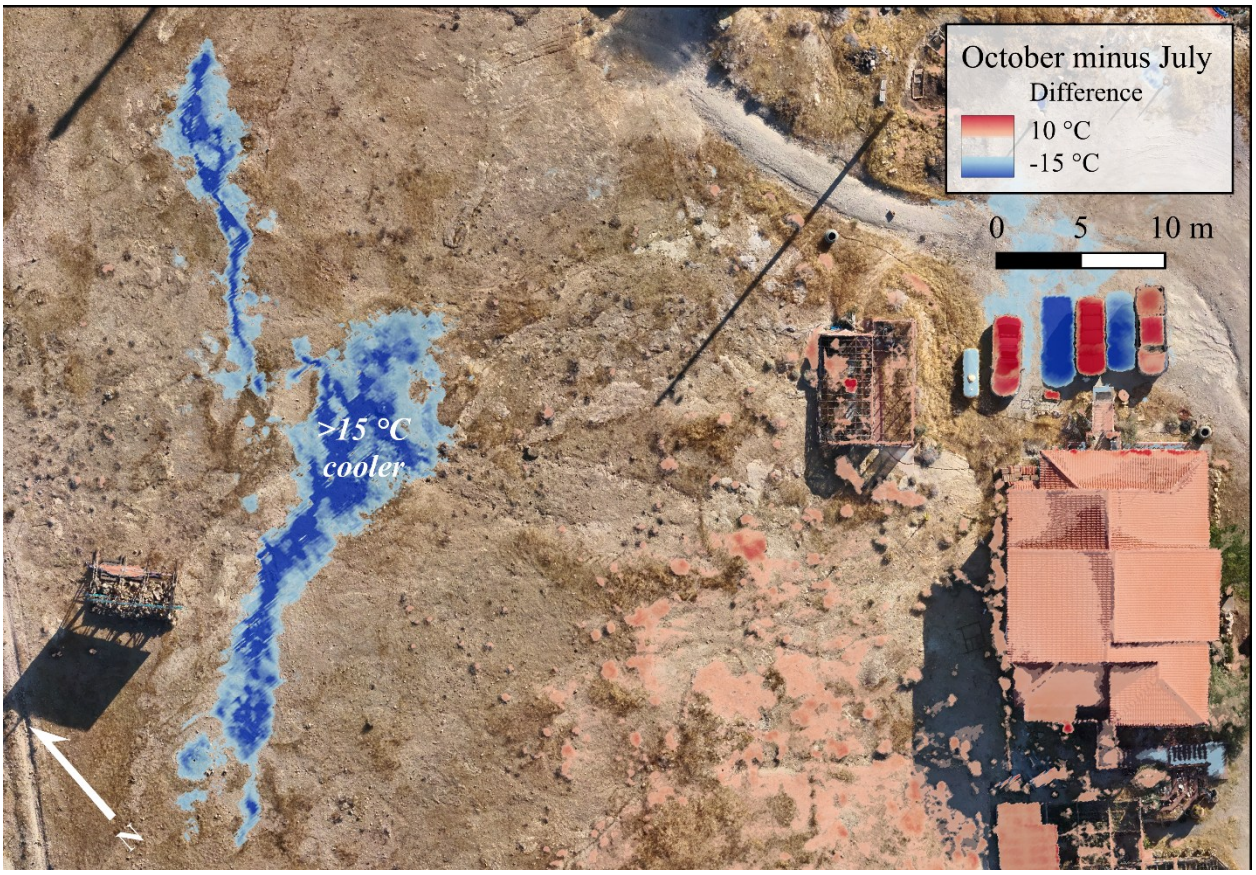

Figure 6. Temperature difference between July and October thermal mosaics near Steamboat Hot Springs Resort. Negative values show areas that were cooler in October than July, including a >15 °C difference in a large area of formerly steaming ground. Base imagery is extracted from ~2 cm /pixel visible light orthomosaic collected in July. Vehicles that were parked in the July acquisition show up as hotter in October because metal typically reads colder than ambient conditions in thermal drone imagery.

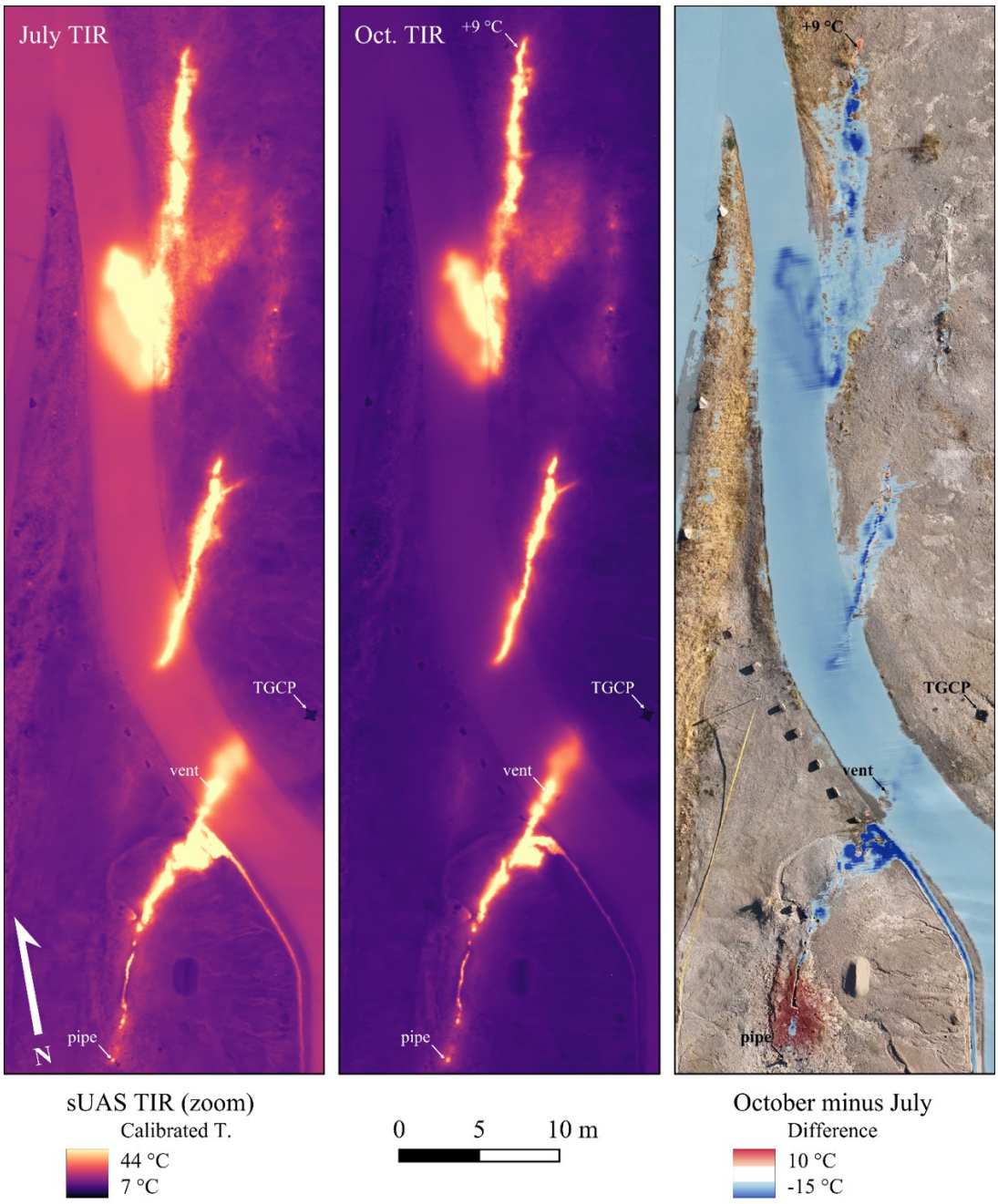

Figure 7. Portions of tuned, orthorectified thermal mosaics showing the area around the geysering pipe and an en echelon array of steaming fissures and warm ground in July and October. The third panel shows differences between the two rasters. Despite the change in seasons, ambient temperatures were similar during both flights. However, increased cloud cover in October resulted in less solar heating of the paved road, leading to the cooler swath in the differencing map. The fissures are generally cooler in October, except for the northern tips of the middle and northern fissures. Some interference along the fissures is likely due to registration errors associated with small (<15 cm) targets.

5.3 Aqueous Geochemistry

5.3.1 Stable Isotopes

Stable isotope compositions for both samples plot away from the local meteoric water line and are consistent with evolved geothermal fluids rather than shallow meteoric groundwater. The geyser-pipe sample (SBG001) and runoff-channel sample (SBG002) cluster closely together on the δ^2H–$\delta^{18}O$ diagram (Figure 8), indicating a shared fluid source. Both samples exhibit a positive $\delta^{18}O$ shift relative to meteoric water, consistent with high-temperature water–rock interaction and exchange within a deep hydrothermal reservoir.

5.3.2 Water-Type Classification

Major anion chemistry plotted on the Cl–SO_4–HCO_3 ternary diagram classifies both samples as chloride waters (Figure 8). Chloride strongly dominates over sulfate and bicarbonate in both samples, placing them within the mature geothermal water field and distinct from steam-heated acid-sulfate or peripheral bicarbonate waters. The two samples plot in close proximity, further supporting a common source fluid with minimal chemical modification between the discharge point and the runoff channel.

5.3.3 Major and Trace Element Chemistry

Both samples exhibit chemical compositions characteristic of deeply sourced geothermal fluids (Table 5). Major-ion chemistry is dominated by sodium and chloride, with Na concentrations of 597–704 mg/L and Cl concentrations of 638–913 mg/L, defining a Na–Cl water type. Magnesium and calcium concentrations are low (Mg 0.13–0.17 mg/L; Ca 4.8–6.5 mg/L), consistent with extensive high-temperature water–rock equilibration and limited mixing with shallow groundwater.

Alkalinity is elevated (660–905 mg/L as $CaCO_3$), and dissolved silica concentrations are high (105–115 mg/L as Si), both typical of prolonged interaction with reservoir rocks at elevated temperature. Trace elements commonly enriched in geothermal systems are present at elevated concentrations, including boron (34–40 mg/L) and lithium (5.8–7.0 mg/L). Arsenic (1.75–2.04 mg/L) and antimony (7.0–8.2 mg/L) are also detected. Nitrate concentrations are below detection (<0.1 mg/L as N) in both samples, indicating minimal influence from shallow surface or anthropogenic sources.

The geyser-pipe and runoff-channel samples show closely similar major- and trace-element signatures, with differences primarily in absolute concentrations rather than relative proportions, consistent with minor dilution or cooling during surface flow rather than distinct fluid origins.

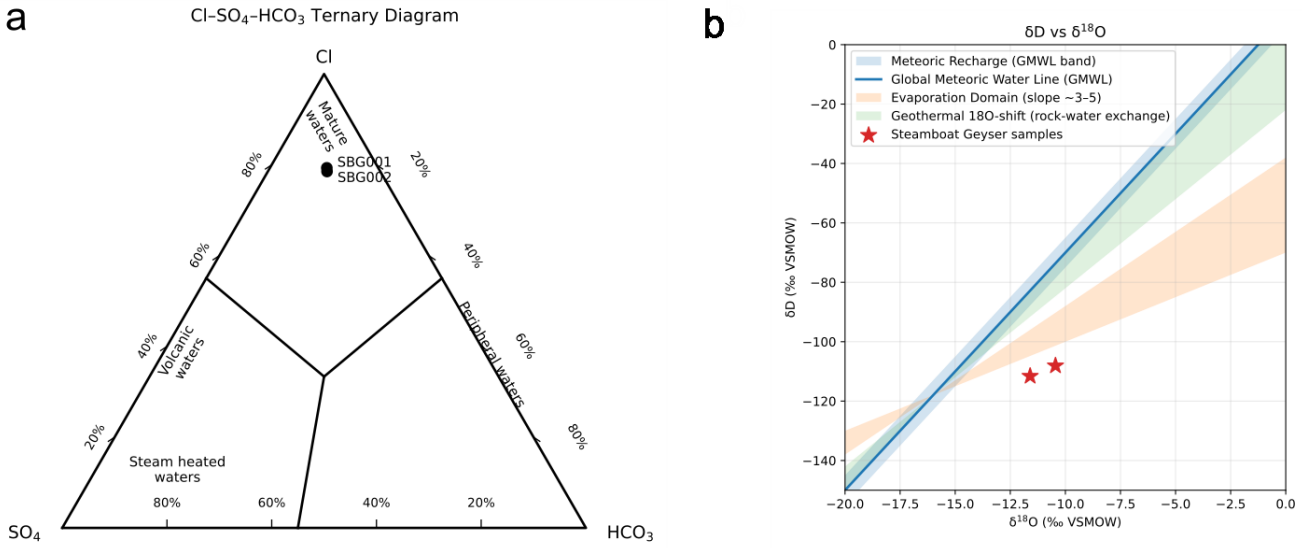

Figure 8. (a) Cl–SO_4–HCO_3 ternary diagram showing major anion chemistry of Steamboat water samples. (b) δD versus $\delta^{18}O$ plot of the same samples with the Global Meteoric Water Line and reference fields shown for context.

Table 5. Select aqueous geochemistry from samples at the lower sinter terrace

Sample	pH	Conductivity (µS/cm)	TDS (mg/L)	Na (mg/L)	K (mg/L)	Ca (mg/L)	Mg (mg/L)	Cl (mg/L)	SO4 (mg/L)	Alkalinity (mg/L as HCO3)	Si (mg/L)	B (mg/L)	Li (mg/L)	As (µg/L)
SBG001	8.9	3660	2300	704	53.6	6.49	0.166	913	153	215	114.5	40200	6990	2040
SBG002	8.8	2620	1720	597	45.3	4.83	0.13	638	112	158	105.5	34100	5840	1750

6. DISCUSSIONS

The recent increase in surface hydrothermal activity at Steamboat highlights the need for sustained, repeat monitoring to document system evolution and to distinguish natural variability from changes associated with shallow pressure redistribution or evolving permeability pathways. Experience from other geothermal fields demonstrates that systematic observation of surface features, fluid chemistry, and subsurface thermal and pressure conditions provides critical context for interpreting changes in hot spring and geyser behavior and for guiding responsible resource management (Allis and Larsen, 2012; Kreuzer et al., 2024; Simmons et al., 2025).

Calibrated seasonal thermal drone surveys with persistent spatial control provide efficient, high-resolution mapping of steaming ground, discharge locations, and temperature anomalies, providing reliable detection of spatial and temporal changes in surface heat flux. Repeat geochemical sampling, including major ions, stable isotopes, and dissolved gases, enables identification of fluid source, mixing relationships, and the relative contributions of deep reservoir fluids versus shallow or steam-heated waters.

Expansion of the temperature monitoring network to include sensors at multiple depths would further constrain vertical heat transport and shallow pressure conditions. Multi-depth temperature and pressure measurements have proven effective in other geothermal systems for detecting subtle subsurface changes that precede or accompany shifts in surface discharge (Simmons et al., 2025). Similarly, recent efforts to standardize surface-thermal-feature management emphasize that integrated monitoring of surface manifestations together with subsurface thermal, hydrologic, and geochemical datasets provides the most reliable framework for protecting and managing active hydrothermal systems (Kreuzer et al., 2024).

Continued implementation of these approaches at Steamboat will establish a quantitative baseline against which future changes can be evaluated and will support early identification of evolving hydrothermal behavior.

7. ACKNOWLEDGEMENTS

We thank Gene Savoy and the staff of Steamboat Springs Resort for site access and logistical support, and Phil Busick for land access and assistance. This work was supported in part by internal research funds from the Nevada Bureau of Mines and Geology, provided by Simon Jowitt and Jim Faulds.

REFERENCES

Allis, R., and Larsen, G.: Roosevelt Hot Springs geothermal field, Utah—reservoir response after more than 25 years of power production, Proceedings, 37th Workshop on Geothermal Reservoir Engineering, Stanford University, Stanford, CA (2012).

Brailo, C., Churchill, M., Bechtold, T., Blake, K., and Zuza, R.: Small unoccupied aerial systems (UAS) and thermal cameras in geothermal exploration and operational fields; a review of UAS equipment and case study at Brady Geothermal Field, Nevada USA, Proceedings, 50th Workshop on Geothermal Reservoir Engineering, Stanford University, Stanford, CA (2024).

Callahan, O.A., and Hart-Wagoner, N.: Applications and limitations of drone-based thermography in geothermal exploration, characterization, and monitoring, Geothermal Resources Council Transactions, 49, (2025).

Faulds, J.E., Henry, C.D., and Hinz, N.H.: Structural controls on geothermal systems in the northwestern Great Basin, Geothermal Resources Council Transactions, 29, (2005), 353–358.

Harvey, M.C., Rowland, J.V., and Luketina, K.M.: Drone with thermal infrared camera provides high-resolution georeferenced imagery of the Waikite geothermal area, New Zealand, Journal of Volcanology and Geothermal Research, 325, (2016), 61–69.

Huntington, J.M.: Hydrothermal alteration mapping using hyperspectral remote sensing at Steamboat Springs, Nevada, Geothermal Resources Council Transactions, 34, (2010).

Irujo, P.G.: IRimage: open-source software for processing images from infrared thermal cameras, PeerJ Computer Science, 8, (2022), e977.

Jayko, A.S.: The Walker Lane: an incipient transform fault along the eastern margin of the Sierra Nevada, California and Nevada, U.S. Geological Survey (2012).

Kreuzer, R., Rockhold, M., Duberstein, C., He, B., Diraddo, S., Steeves, T., and Simmons, S.: Hot Springs and Geysers: exploring historical and modern impacts of geothermal energy production on surface thermal features and standardizing management practices, Geothermal Rising Conference Transactions, 48, (2024).

Müller, D., Walter, T.R., Zimmer, M., and Gonzalez, G.: Distribution, structural and hydrological control of the hot springs and geysers of El Tatio, Chile, revealed by optical and thermal infrared drone surveying, Journal of Volcanology and Geothermal Research, 432, (2022).

Pavlis, T.L., and Mason, K.A.: The new world of 3D geologic mapping, GSA Today, 27, (2017), 4–10.

Silberman, M.L., White, D.E., Keith, T.E.C., and Dockter, R.D.: Duration of hydrothermal activity at Steamboat Springs, Nevada, U.S. Geological Survey Professional Paper 458-D (1979).

Siler, D.L.: Structural controls and play-fairway analysis of geothermal resources in the Great Basin, Geothermal Resources Council Transactions, (2017).

Simmons, S.F., Rockhold, M.L., and Kreuzer, R.: Sustaining hot spring activity in the vicinity of geothermal developments, Proceedings, 50th Workshop on Geothermal Reservoir Engineering, Stanford University, Stanford, CA (2025).

Skalbeck, J.D., Shevenell, L.A., and Calvin, W.M.: Hyperspectral remote sensing of geothermal alteration minerals at Steamboat Springs, Nevada, Geothermal Resources Council Transactions, 26, (2002).

Westoby, M.J., Brasington, J., Glasser, N.F., Hambrey, M.J., and Reynolds, J.M.: Structure-from-motion photogrammetry: a low-cost, effective tool for geoscience applications, Geomorphology, 179, (2012), 300–314.

White, D.E.: Hydrology, activity, and heat flow of the Steamboat Springs thermal system, Washoe County, Nevada, U.S. Geological Survey Professional Paper 458-C (1968).

White, D.E., Thompson, G.A., and Sandberg, C.A.: Rocks, structure, and geologic history of Steamboat Springs thermal area, Washoe County, Nevada, U.S. Geological Survey Professional Paper 458-B (1964).